Analysis of the Turkel–Zwas Scheme
for the Shallow-Water Equations

B. NETA

*Department of Mathematics, Naval Postgraduate School,
Monterey, California 93943*

AND

I. M. NAVON*

*Department of Mathematics and Supercomputer Computations Research Institute,
Florida State University, Tallahassee, Florida 32306*

A transfer function analysis is used to analyze the Turkel–Zwas explicit large time step scheme applied to the shallow-water equations. The transfer function concept leads to insight into the behavior of this discretization scheme in terms of comparison between continuous and discrete amplitude, phase, and group velocity coefficients. The dependence of the distortion increases with the increase in the time-step size taken for the Turkel–Zwas scheme, which depends on the ratio between a coarse and a fine mesh. A comparison with earlier results of Schoenstadt (Naval Post-Graduate School Report NPS-53-79-001, 1978 (unpublished)) shows the Turkel–Zwas scheme to give reasonable results up to time steps three times larger than the CFL limit.   © 1989 Academic Press, Inc.

1. INTRODUCTION

The transfer function approach introduced by Schoenstadt [7, 8] has been used by him to study the behavior of the semi-discrete shallow water equations discretized with different staggered and unstaggered finite-difference grid arrangements for dispersion and geostrophic adjustment properties.

The use of the transfer function approach leads to important insights into the differences caused by various discretization schemes, differences that do not directly emerge from phase propagation considerations alone.

In the present paper we apply the transfer function approach to the Turkel–Zwas explicit large time-step scheme for the shallow-water (S-W) equations (Navon and de Villiers, [6]).

This scheme proposes treating terms associated with the fast gravity inertia waves on a coarser grid (but to a higher accuracy) than the terms associated with the slow Rossby waves. The relationship between the coarse and fine meshes is an integer

277

$p > 1$, thus allowing with little additional work time steps nearly p times larger than those allowed by the usual explicit stability criteria for the shallow water equations.

The particular model we shall use is based on the linearized 1-dimensional shallow water equations model without mean flow, which is the same model used by Schoenstadt [8], Arakawa and Lamb [1] and others.

Our analysis of the Turkel–Zwas discretization of space derivatives will study the effect of transients introduced by the particular discretization used and their effects for different coarse-to-fine mesh ratios in comparison with the differential case. In the next section we first present the salient features of the Turkel–Zwas scheme as applied by Navon and de Villiers [6] in the Cartesian β-plane case of the S-W equations (see Appendix B for definitions). In Section 3 we detail the transfer function analysis of the semi-discrete, finite-difference Turkel–Zwas scheme as well as that of the (continuous) differential case, and the amplitude coefficients of the discretized approximate filters are derived.

In Section 4 the numerical and graphical results of the transfer function analysis of the Turkel–Zwas scheme are compared to the transfer functions analysis of the differential model in as far as amplitude coefficients of the discretized approximate filters, phase, and group velocities. The effect of distortion between the continuous and discrete case for various wavelengths and time steps determined by the coarse-to-fine mesh ratio p and their implications for numerical modeling will be also discussed. In Section 5 the process of geostrophic adjustment (Haltiner and Williams [4, pp. 45–52]) (see also Appendix B) for the Turkel–Zwas scheme will be discussed.

Finally in Section 6 some topics of further research are discussed.

2. THE TURKEL–ZWAS EXPLICIT LARGE TIME STEP SCHEME FOR THE SHALLOW-WATER EQUATIONS

We shall deal only with the Cartesian case of the shallow-water equations in a channel on a rotating earth, i.e.,

$$u_t + uu_x + vu_y + gh_x - fv = 0,$$

$$v_t + uv_x + vv_y + gh_y + fu = 0, \tag{1}$$

$$h_t + (hu)_x + (hv)_y = 0,$$

where u and v are the velocity components in the x and y directions, respectively; f is the Coriolis parameter given by the β-plane approximation

$$f = \hat{f} + \beta(y - D/2), \tag{2}$$

where D is the width of the channel with $\hat{f}$ and β constants, h is the depth of the fluid, and g is the acceleration of gravity. Here $0 < x \leqslant L$, $0 \leqslant y \leqslant D$, $t \geqslant 0$, where L is the length of the channel. For a description of the boundary conditions see Navon and Riphagen [22].

The Turkel–Zwas scheme, which is a space-splitting scheme takes the form of the following generalized leapfrog method (see [9; 6])

$$u_{i,j}^{n+1} = u_{i,j}^{n-1} - \lambda \left[u_{i,j}^n (u_{i+1,j}^n - u_{i-1,j}^n) + v_{i,j}^n (u_{i,j+1}^n - u_{i,j-1}^n) \right.$$
$$\left. + \frac{g}{p} (h_{i+p,j}^n - h_{i-p,j}^n) \right] + 2 \Delta t f \left[(1-\alpha) v_{i,j}^n + \frac{\alpha}{2} (v_{i+p,j}^n - v_{i-p,j}^n) \right],$$

$$v_{i,j}^{n+1} = v_{i,j}^{n-1} - \lambda \left[u_{i,j}^n (v_{i+1,j}^n - v_{i-1,j}^n) + v_{i,j}^n (v_{i,j+1}^n - v_{i,j-1}^n) \right.$$
$$\left. + \frac{g}{p} (h_{i,j+p}^n - h_{i,j-p}^n) \right] - 2 \Delta t f \left[(1-\alpha) u_{i,j}^n + \frac{\alpha}{2} (u_{i,j+p}^n - u_{i,j-p}^n) \right], \tag{3}$$

$$h_{i,j}^{n+1} = h_{i,j}^{n-1} - \lambda \left[u_{i,j}^n (h_{i+1,j}^n - h_{i-1,j}^n) + v_{i,j}^n (h_{i,j+1}^n - h_{i,j-1}^n) \right.$$
$$\left. + \frac{h_{i,j}^n}{p} (u_{i+p,j}^n - u_{i-p,j}^n + v_{i,j+p}^n - v_{i,j-p}^n) \right],$$

where

$$u_{i,j}^n = u(i \Delta x, j \Delta y, n \Delta t), \qquad \lambda = \frac{\Delta t}{\Delta x} = \frac{\Delta t}{\Delta y},$$

and $p > 1$ is an integer which defines the relationship between the coarse mesh on which terms associated with the inertia-gravity waves are treated and the fine mesh on which terms associated with the slow Rossby waves are discretized.

It has been proven (see Navon and de Villers, [6]) that the stability criterion for this scheme is

$$\frac{\Delta t}{\Delta x} \leqslant \frac{1}{|u| + |v| + \sqrt{2gh/p}} \tag{4}$$

and, since for typical atmospheric conditions,

$$\sqrt{gh} \gg (|u| + |v|), \tag{5}$$

one can use time steps nearly p times larger than allowed by the CFL condition for the usual explicit leapfrog scheme.

In (3) we use $\alpha = \frac{1}{3}$, which gives a compact fourth-order accurate finite-difference approximation for the terms of the coarse mesh (see [6]).

The Turkel–Zwas scheme has been applied by Turkel and Zwas [9] on both Cartesian and spherical grids while Navon and deVilliers [6] have applied it to a real data hemispheric barotropic model with constraint restoration. Jespersen [5] has applied a similar scheme. As this method is the counterpart of the split-explicit

method of Gadd [2; 3] there is considerable interest to study its impact on the geostrophic adjustment process in the S-W equations as well as to be able to assess the effect of this discretization on the amplitude and phase distortion characteristics.

3. A TRANSFER-FUNCTION ANALYSIS OF THE TURKEL–ZWAS SCHEME APPLIED TO THE SHALLOW-WATER EQUATIONS

We will use here the transfer function approach applied to the linearized, 1-dimensional shallow-water equations with no mean flow, in an infinite region

$$\frac{\partial u}{\partial t} - fv + g\frac{\partial h}{\partial x} = 0,$$

$$\frac{\partial v}{\partial t} + fu = 0, \tag{6}$$

$$\frac{\partial h}{\partial t} + H\frac{\partial u}{\partial x} = 0,$$

where u denotes the perturbation velocity in the x direction, v the perturbation velocity normal to the x direction, H and h the mean and perturbed heights of the free surface, respectively, g the acceleration of gravity, and f the Coriolis parameter.

For the continuous analysis we will refer to the results of Schoenstadt [7; 8].

3.1. The Transfer Function Analysis of the Turkel–Zwas Scheme

The discrete form of the Turkel–Zwas scheme is

$$\frac{\partial u_i}{\partial t} = -\frac{g}{2p\,\varDelta x}(h_{i+p} - h_{i-p}) + f\left[(1-\alpha)v_i + \frac{\alpha}{2}(v_{i+p} + v_{i-p})\right],$$

$$\frac{\partial v_i}{\partial t} = -fu_i, \tag{7}$$

$$\frac{\partial h_i}{\partial t} = \frac{-H}{2p\,\varDelta x}(u_{i+p} - u_{i-p}).$$

If we Fourier transform this system using

$$\int_{-\infty}^{+\infty} u(x + \varDelta x, t)\, e^{-ikx}\, dx = e^{ik\,\varDelta x}\hat{u}(k, t), \tag{8}$$

where we denote Fourier transforms by an overlying hat we obtain

$$\frac{\partial \hat{u}}{\partial t} = \frac{-g}{2p\,\varDelta x}\hat{h}(k, t)[e^{ikp\varDelta x} - e^{-ikp\varDelta x}] + f\hat{v}\left[(1-\alpha) + \frac{\alpha}{2}(e^{ikp\varDelta x} + e^{-ikp\varDelta x})\right] \tag{9}$$

or

$$\frac{\partial \hat{u}}{\partial t} = \frac{-g}{2p\,\Delta x}\,\hat{h}(k,\,t)\,2i\sin kp\,\Delta x + f\hat{v}[(1-\alpha)+\alpha\cos kp\,\Delta x] \tag{10}$$

Finally, the Fourier transformed system is

$$\frac{\partial \hat{u}_i}{\partial t} = -ig\sigma\hat{h}_i + f\rho\hat{v}_i,$$

$$\frac{\partial \hat{v}_i}{\partial t} = -f\hat{u}_i, \tag{11}$$

$$\frac{\partial \hat{h}_i}{\partial t} = -iH\sigma\hat{u}_i,$$

where

$$\sigma = \frac{\sin kp\,\Delta x}{p\,\Delta x}, \tag{12}$$

$$\rho = \frac{2+\cos kp\,\Delta x}{3}. \tag{13}$$

While (10) refers to a general α, (13) assumes $\alpha = \frac{1}{3}$. Let

$$\begin{pmatrix} \hat{u} \\ \hat{v} \\ \hat{h} \end{pmatrix} = e^{ivt}\begin{pmatrix} \hat{u}_0(k) \\ \hat{v}_0(k) \\ \hat{h}_0(k) \end{pmatrix}; \tag{14}$$

by substituting (14) into (11) we obtain

$$iv\hat{u}_0 - \rho f\hat{v}_0 + ig\sigma\hat{h}_0 = 0,$$
$$f\hat{u}_0 + iv\hat{v}_0 = 0, \tag{15}$$
$$iH\sigma\hat{u}_0 + iv\hat{h}_0 = 0.$$

By solving the determinant of (15) we obtain three eigenvalues

$$v = 0 \tag{16}$$

and

$$v = \pm\sqrt{\rho f^2 + Hg\sigma^2}. \tag{17}$$

By an eigenvalue/eigenvector approach, we get the eigenvectors corresponding to these eigenvalues.

It is easy to see that

$$\hat{u} = \frac{1}{2}\left(\hat{u}_0 - \frac{i\rho f}{v}\hat{v}_0 - \frac{g\sigma}{v}\hat{h}_0\right)e^{ivt} + \frac{1}{2}\left(\hat{u}_0 + \frac{i\rho f}{v}\hat{v}_0 + \frac{g\sigma}{v}\hat{h}_0\right)e^{-ivt},$$

$$\hat{v} = \frac{f}{v^2}ig\sigma\hat{h}_0 - \frac{iH\sigma}{v^2}ig\sigma\hat{v}_0 + \frac{if\rho}{2v^2}\left((v\hat{u}_0 - i\rho f\hat{v}_0 - g\sigma\hat{h}_0)e^{ivt}\right.$$

$$\left. - \frac{-if\rho}{2v^2}(v\hat{u}_0 + i\rho f\hat{v}_0 + g\sigma\hat{h}_0)e^{-ivt}, \right.$$ (18)

$$\hat{h} = \frac{f^2\rho}{2v^2}\hat{h}_0 - \frac{i\rho fH\sigma}{v^2}\hat{v}_0 - (v\hat{u}_0 - i\rho f\hat{v}_0 - g\sigma\hat{h}_0)\frac{H\sigma}{2v^2}e^{ivt}$$

$$+ \frac{H\sigma}{2v^2}(v\hat{u}_0 + i\rho f\hat{v}_0 + g\sigma\hat{h}_0)e^{-ivt},$$

where $\hat{u}_0$, $\hat{v}_0$, and $\hat{h}_0$ are the Fourier transforms of the initial condition,

$$v = f\sqrt{\rho + \lambda^2\sigma^2}$$ (19)

$$\lambda^2 = gH/f^2 = L_R^2,$$ (20)

where $\lambda \equiv L_R$ is the Rossby radius of deformation (see, e.g., [4, pp. 45–52] and Appendix B).

Collecting terms we find, finally,

$$\hat{u} = \hat{u}_0 \cos vt + \frac{\rho f}{v}\hat{v}_0 \sin vt - \frac{ig\sigma}{v}\hat{h}_0 \sin vt,$$

$$\hat{v} = \frac{gH\sigma^2}{v^2}\hat{v}_0 + \frac{igf\sigma}{v^2}\hat{h}_0 - \frac{f\rho}{v}\hat{u}_0 \sin vt + \frac{\rho^2 f^2}{v^2}\hat{v}_0 \cos vt$$

$$- \frac{ig\sigma\rho f}{v^2}\hat{h}_0 \cos vt,$$ (21)

$$\hat{h} = -\frac{i\rho fH\sigma}{v^2}\hat{v}_0 + \frac{\rho f^2}{v^2}\hat{h}_0 - \frac{iH\sigma}{v}\hat{u}_0 \sin vt$$

$$+ \frac{i\rho fH\sigma}{v^2}\hat{v}_0 \cos vt + \frac{gH\sigma^2}{v^2}\hat{h}_0 \cos vt,$$

so that Eq. (21) tends to Eq. (11) in Schoenstadt [7].

Each transform field can be written as the sum of a steady-state part (denoted by s subscript) and a transient part, see [4, p. 49]. In this case the steady part is

$$\hat{u}_s = 0,$$

$$\hat{v}_s = \hat{v}_0 - \frac{1}{\rho + \lambda^2\sigma^2}\left(\rho\hat{v}_0 - \frac{ig\sigma}{f}\hat{h}_0\right),$$ (22)

$$\hat{h}_s = \hat{h}_0 - \frac{H}{f}\frac{i\sigma}{\rho + \lambda^2\sigma^2}\left(\rho\hat{v}_0 - \frac{ig\sigma}{f}\hat{h}_0\right).$$

The steady-state solution in the continuous case is given by (see [7])

$$\hat{u}_s = 0,$$

$$\hat{v}_s = \hat{v}_0 - \frac{f^2}{f^2 + k^2gH}\left[\hat{v}_0 - \frac{ikg}{f}\hat{h}_0\right],$$ (23)

$$\hat{h}_s = \hat{h}_0 - \frac{H}{f}\frac{f^2}{f^2 + k^2gH}ik\left[\hat{v}_0 - \frac{ikg}{f}\hat{h}_0\right].$$

Comparison of (21) and (19) with the continuous differential case (see [8]) shows that the main changes of the Turkel–Zwas semi-discretization are:

1. The filter coefficients $1/v$, k/v, and k^2/v^2 are replaced respectively by ρ/v, σ/v, and σ^2/v^2.

2. The filter coefficient $1/v^2$ is replaced by ρ^2/v^2 except in one case where we have ρ/v^2.

3. The filter coefficient k/v^2 is replaced by $\rho\sigma/v^2$ except in one case where we have σ/v^2.

4. The phase velocity $f\sqrt{1 + \lambda^2k^2}/k$ is replaced by $f\sqrt{\rho + \lambda^2\sigma^2}/k$.

Note that σ^2/v^2 and ρ^2/v^2 are squares of filter coefficients and will not be plotted.

In order to get the semi-discrete steady-state solution in the physical space we have to calculate inverse transforms. It is useful for this purpose to employ the convolution theorem which may be written

$$\frac{1}{2\pi}\int_{-\infty}^{+\infty}\hat{F}(K)\,\hat{G}(k)\,e^{ikx}\,dk = \int_{-\infty}^{+\infty}F(x')\,G(x - x')\,dx,$$ (24)

where $\hat{F}$ and $\hat{G}$ are the transforms of F and G.

It is easily shown that

$$\frac{i\sigma g}{f}\hat{h}_0 - \rho\hat{v}_0 = \mathscr{F}\left\{\frac{g}{f}\frac{h(x + p\,\Delta x, 0) - h(x - p\Delta x, 0)}{2p\,\Delta x}\right.$$

$$\left. - \frac{2}{3}v(x, 0) - \frac{1}{6}\left[v(x + p\Delta x, 0) + v(x - p\,\Delta x, 0)\right]\right\},$$ (25)

where $\mathscr{F}$ denotes the Fourier transform. Let

$$\hat{d}(x, 0) = \frac{2}{3} v(x, 0) + \frac{1}{6} \left[(x + p\, \Delta x, 0) + v(x - p\, \Delta x, 0) \right]$$

$$- \frac{g}{f} \frac{h(x + p\, \Delta x, 0) - h(x - p\, \Delta x, 0)}{2p\, \Delta x} \tag{26}$$

denote the initial geostrophic departure analog for the Turkel–Zwas scheme (i.e., the departure from geostrophic balance) defined analytically as

$$d(x, t) = v(x, t) - gf^{-1} \frac{\partial h}{\partial x}(x, t). \tag{27}$$

Thus if we can invert $i\sigma/(\rho + \lambda^2 \sigma^2)$ and $1/(\rho + \lambda^2 \sigma^2)$ (see Appendix A), then the steady-state solution would be available by convolution,

$$u_s(x) = 0, \tag{28}$$

$$v_s(x) = v(x, 0) - p\, \Delta x \sum_{n=-\infty}^{\infty} \left\{ \frac{e^{-\beta_1 |2np\, \Delta x|/\lambda}}{\sinh \xi_1} \frac{1}{\theta} + \frac{1}{2-\theta} \frac{e^{-\beta_2 |2np\, \Delta x|/\lambda}}{\sinh \xi_2} \right\} \hat{d}(x - 2np\, \Delta x, 0),$$
$$\tag{29}$$

$$h_s(x) = h(x, 0) - \frac{3H}{f} \sum_{n=-\infty}^{\infty} \left\{ \frac{e^{-\beta_1 |2np\, \Delta x|/\lambda}}{-\theta} + \frac{e^{-\beta_2 |2np\, \Delta x|/\lambda}}{2-\theta} \right\} \hat{d}(x - 2np\, \Delta x, 0), \tag{30}$$

where

$$\beta_1 = \frac{\lambda}{p\, \Delta x} \xi_1 \tag{31}$$

$$\beta_2 = \frac{\lambda}{p\, \Delta x} (\xi_2 - i\pi). \tag{32}$$

and ξ_1, ξ_2 are given in Appendix A.

Clearly (28)–(30) tend to the corresponding steady-state solution given by (13) in [7] as $\Delta x \to 0$.

The effect of the Turkel–Zwas discretization on the process of geostrophic adjustment is similar to the one obtained by Schoenstadt [7; 8] and Haltiner and Williams [4], i.e.,

(a) The geostrophic departure $d(x, t)$ is converted to a finite-difference measure which depends on the coarse-to-fine mesh ratio p.

(b) The transient disturbances due to initial imbalances, which excite short-wave gravity waves propagating away from the initial region of imbalance, die off exponentially away from the initial region neighborhood. The rate of such decay is

smaller than in the differential case. The rate of decay decreases as $(\Delta x)^2/\lambda^2$ increases. If the initial imbalance has a scale that is small in comparison with the scale of the region, the geostrophic adjustment process operates very efficiently. When those scales are comparable, the fields will oscillate for some time.

The final state depends on $(L/\lambda)^2$. When the scale of the initial field L is small compared to the Rossby radius of deformation, L_R the final state is determined by the rotational part of the initial wind field, wheras when $L > L_R$ the final state is determined by the initial pressure (mass field) (see also Appendix B).

4. Discussion of Numerical Results

In Figs. 1a–1e the amplitude coefficients of the filter of the continuous differential model are displayed. As the solutions are band-limited to the region

$$\frac{-\pi}{d} < k < \frac{\pi}{d},$$

where k is the wavenumber, we display the results as a function kd/π where $d = \Delta x = h$; i.e., the scale starts at long wave numbers and ends up at the shortest resolvable wave $k = \pi/d$ or $kd/\pi = 1$. Since the filter coefficients determine how the energy in the initial disturbance is partitioned into the transient and steady-state fields, then the degree to which discrete filter coefficients resemble the continuous ones can be viewed as an indicator of the degree to which a particular discretization accurately portrays the continuous model energy distribution.

The degree of discrepancy between continuous and corresponding discrete coefficients should be construed as representing a distortion between the continuous and discrete solutions. The amplitude distortion in system (21) is governed in each term by one of the three factors $1/v$, k/v, or k^2/v^2. The terms with coefficient k/v have their high frequencies least affected (high-pass filter) the terms with coefficient $1/v$ have their low frequencies least affected (low-pass filter), and those with coefficient k/v^2 have their frequencies in some middle range least affected (band-pass filter).

In the following table we list the filter weights for the Turkel–Zwas scheme as well as the continuous case.

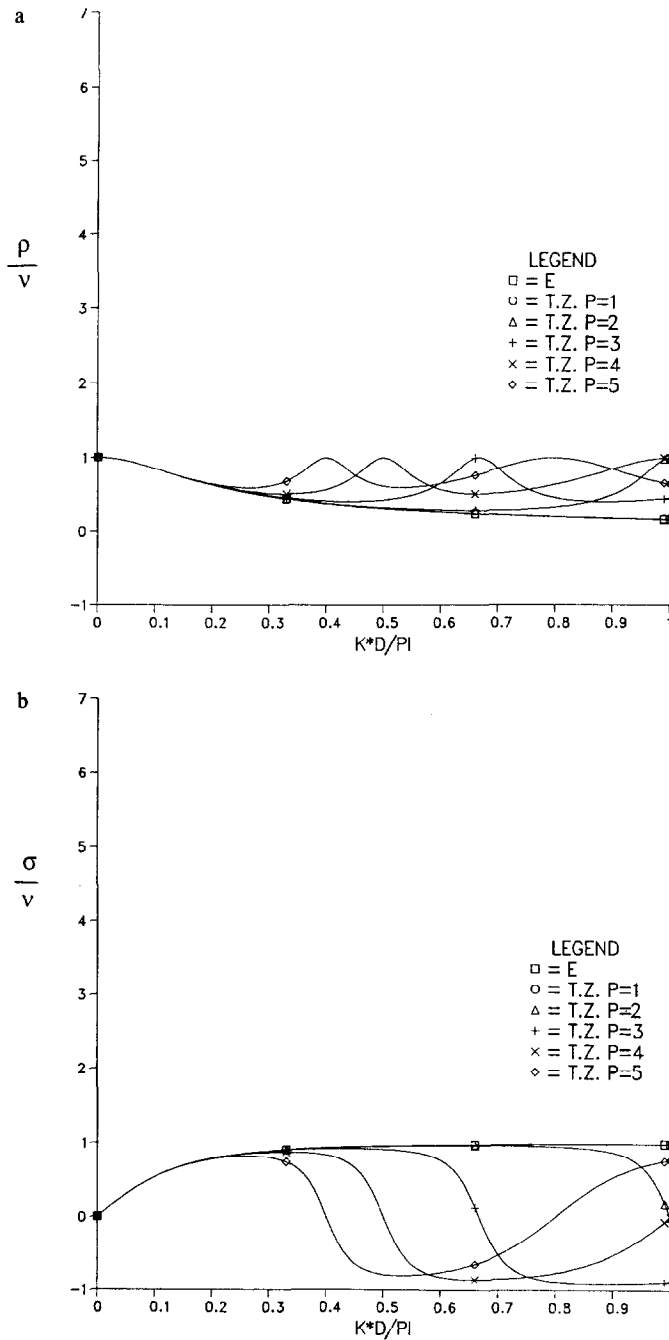| Scheme	Notation	α	ρ	σ
Continuous	E	1	1	k
Turkel–Zwas p	TZP	1	$\dfrac{2 + \cos pk\,\Delta x}{3}$	$\dfrac{\sin kp\,\Delta x}{p\,\Delta x}$

a

b

FIG. 1. (a) The amplitude coefficient ρ/v for the unstaggered Turkel–Zwas scheme for coarse/fine mesh ration $p=1$ to $p=5$ as well as the differential case as a function of kd/π. (b) Same as (a) but for amplitude coefficient σ/v (low-pass filter). (c) Same as (a) but for amplitude coefficient σ/v^2 (band-pass filter). (d) Same as (a) but for amplitude coefficient ρ/v^2. (e) Same as (a) but for amplitude coefficient $\rho\sigma/v^2$.

286

c

$$\frac{\sigma}{v^2}$$

LEGEND
□ = E
○ = T.Z. P=1
△ = T.Z. P=2
+ = T.Z. P=3
× = T.Z. P=4
◇ = T.Z. P=5

K*D/PI

d

LEGEND
□ = E
○ = T.Z. P=1
△ = T.Z. P=2
+ = T.Z. P=3
× = T.Z. P=4
◇ = T.Z. P=5
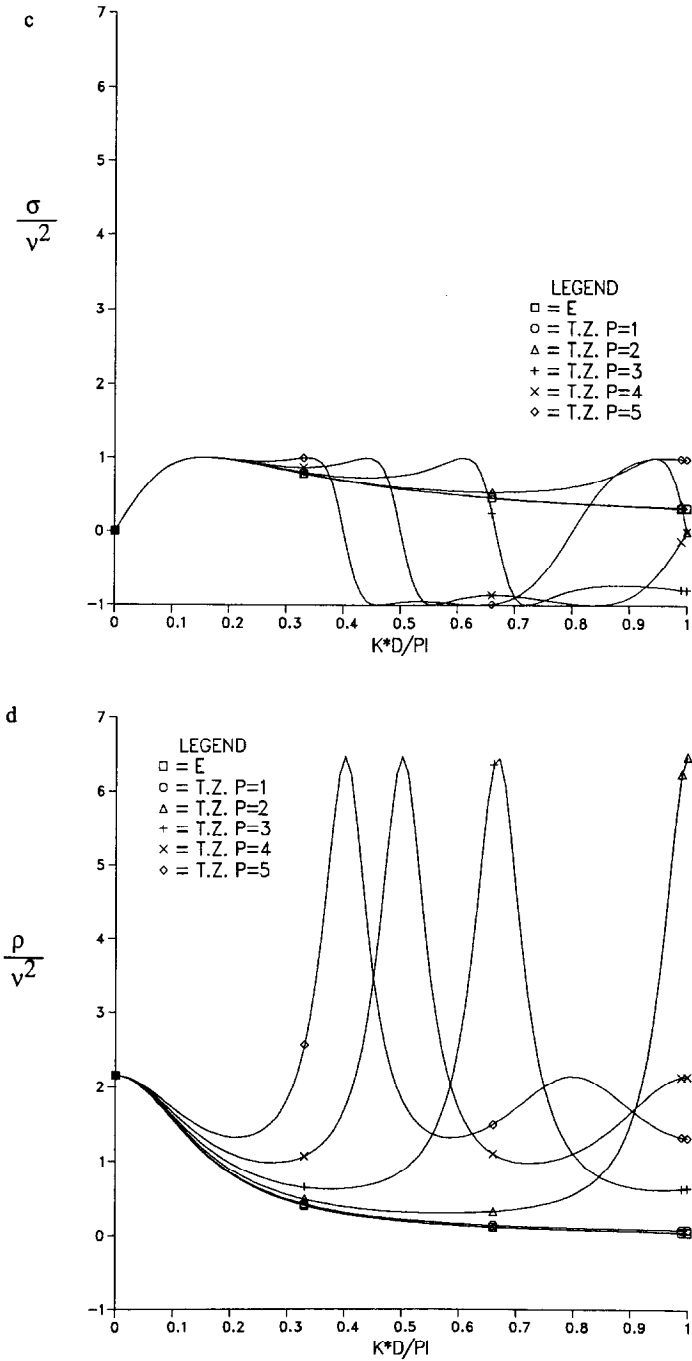
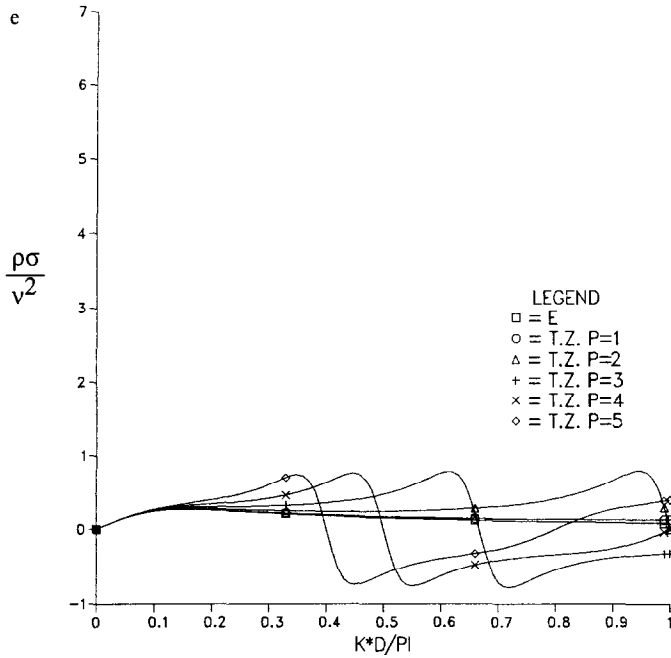$$\frac{\rho}{v^2}$$

K*D/PI

FIG. 1—*Continued.*

FIG. 1—Continued.

The phase speed in these notations is given by

$$\frac{v}{k} = \frac{f}{\alpha k} \sqrt{\rho + \lambda^2 \sigma^2}. \tag{33}$$

The group velocity dv/dk can be computed easily as

$$\frac{dv}{dk} = f \frac{(d\rho/dk + \lambda^2 \sigma(d\sigma/dk))\alpha - (\rho + \lambda^2 \sigma^2)(d\sigma/dk)}{\alpha^2 \sqrt{\rho + \lambda^2 \sigma^2}}. \tag{34}$$

Results for these schemes appear in Schoenstadt [8]. Figures 2a and b show the phase velocity and group velocity for the differential case respectively.

In Fig. 1a we also display the variation of ρ/v for the Turkel–Zwas scheme on an A-grid (see, e.g., [1, p. 181] and Appendix B) with coarse-to-fine mesh ratio p varying from 1 to 5 for a range of wave numbers starting with long wavelengths and ending with the shortest resolvable wavelength. Compared to the A2 case of [8], we get better results (i.e., less departure from the continuous filter) for the case $p = 2$, while the case $p = 3$ behaves like the second-order finite difference approximation of A-grid (A2).

The same can be said for Fig. 1b where we get better results than A2 for $p = 2$ and comparable results for $p = 3$ for σ/v. The deterioration always occurs at shorter wavelength scales.

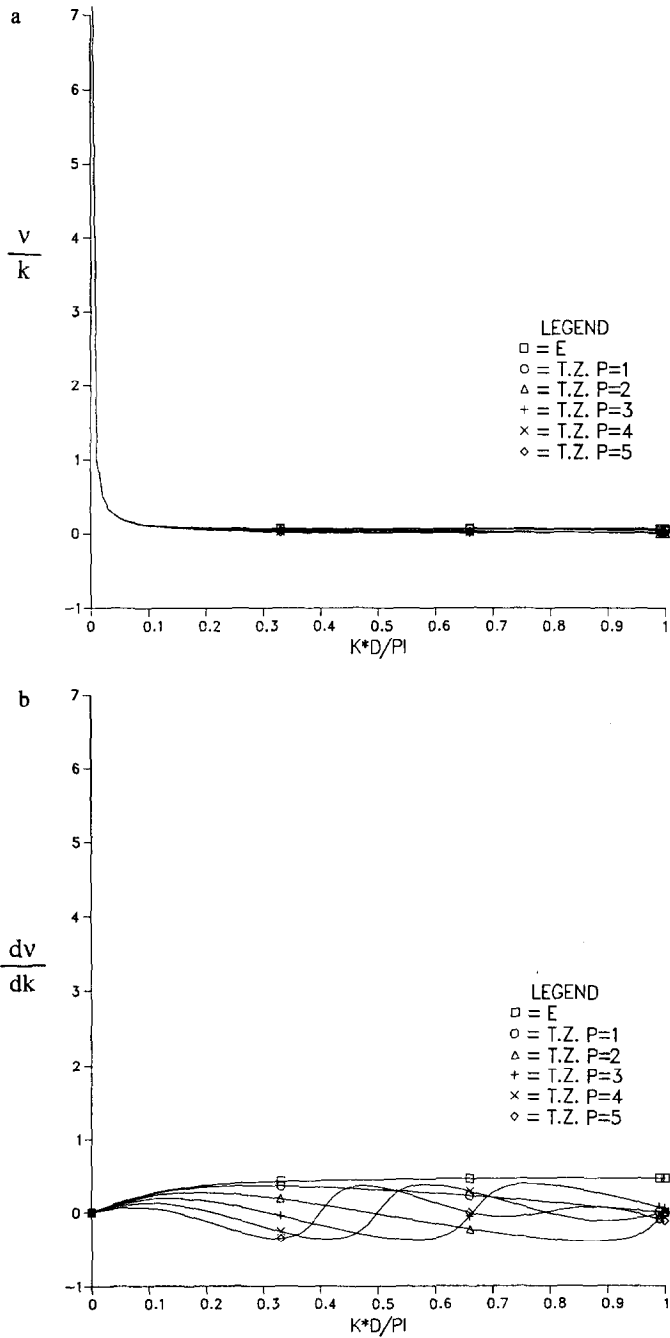FIG. 2. (a) The phase velocity $c = v/k$ for the Turkel–Zwas scheme with different coarse/fine mesh ratios $p = 1, ..., 5$ (i.e., different time steps) as a function of kd/π, displayed against the differential solution of the phase velocity. (b) Group velocity dv/dk as a function of kd/π for the differential case.

289

For σ/v^2 (Fig. 1c), we again observe similar results to A2 for $p = 2$, but worse results than A2 for the Turkel–Zwas scheme with $p = 3$.

Figure 1d depicts the evolution of the amplitude coefficient ρ/v^2. Again worse results than A2 occur for a coarse/fine mesh ratio of $p \geqslant 3$.

Figure 1e depicts the evolution of the amplitude coefficient $\rho\sigma/v^2$ for a range of wave numbers starting with long wavelengths. Results equivalent to A2 occur for a coarse/fine mesh ratio up to $p = 3$.

Figure 2a shows the phase v/k for the continuous coarse as well as for the second-order finite-difference Turkel–Zwas scheme with different p ratios. The case with $p = 2$ is similar to the A2 case while the cases for $p = 3$ to $p = 5$ show an early departure (i.e., occuring at longer wavelengths) from the continuous case but continue to show a rather acceptable behavior.

Figure 2b depicts the group velocity dv/dk for the continuous case as well as for the second-order finite-difference Turkel–Zwas scheme with different p ratios. Again the case $p = 2$ is similar to the A2 case while for higher p ratios a more oscillatory behavior is observed and the departure from the continuous case occurs at longer wavelengths as a function of increasing p.

To summarize, the phase velocities are less than the differential value and the error is largest for the shortest resolvable wave ($\mu = \pi/d$) and for the high values of p, mainly for $p \geqslant 3$.

The group velocities are also too slow for the short waves and tend to become spuriously negative for $p \geqslant 2$, becoming more oscillatory for increasing values of p. Since the energy propagates with the group velocity our result means that short waves will propagate energy in the wrong direction giving a noisy forecast. A nonlinear normal mode initialization (see [4, pp. 377–385]) can alleviate this problem.

Gravity-inertia short waves may arise from geostropic adjustment after initialization, from small-scale heating, from nonlinear interactions, or from mountain effects.

As shown by Schoenstadt [8] and Arakawa and Lamb [1], the short-wave structure will be better simulated by staggered-grid arrangements of the dependent variables, in particular, by schemes B or C of Arakawa (see [1, p. 181]). To obtain similar small-scale short-wave structure with the unstaggered grid scheme A, a smaller grid size is required as well as additional smoothing. Our results for the Turkel–Zwas scheme show that reasonable results are obtained up to $p = 3$ using the Turkel–Zwas scheme with an unstaggered grid arrangement (the Arakawa A scheme).

5. Geostrophic Adjustment for the Turkel–Zwas Scheme

In the atmosphere a geostrophic balance exists between the Coriolis *force* and the pressure gradient force when the atmosphere is modeled by the meteorological primitive equations of which the shallow-water equations are a particular case. This balance is contained in a dispersive wave equation.

If imbalances occur in the initial conditions, the atmosphere modeled by the primitive equations reacts to the imperfect initial conditions by the dipersive wave mechanism and moves toward a geostrophic balance in a process referred to as *geostrophic adjustment* (see Appendix B).

In fact, this adjustment process operates continually to keep the atmosphere in a state of approximate geostrophic balance.

The steady-state solution Eq. (22) for the Turkel–Zwas scheme represents a distortion in a state of geostrophic balance with a new frequency given by Eq. (19) to be compared to the differential frequency

$$v = (f^2 + k^2 hH)^{1/2} \tag{35}$$

as obtained in [7].

6. Conclusions

We have used a transfer function approach to examine the shallow-water equations discretized by the second-order unstaggered space-splitting Turkel–Zwas scheme which allows the use of time-steps larger than those permitted by the CFL condition.

The results show that for coarse-to-fine mesh ratios of up to $p = 3$, we obtain results similar to second-order finite difference scheme A results given in [7; 8], pointing to the fact that we can use the Turkel–Zwas scheme with time steps up to three times larger than the explicit CFL condition allows. The results point out distortions in the process of geostrophic adjustment which increase with increasing p. The results of this 1-dimensional analysis also show (see Fig. 2b) that the Turkel–Zwas scheme for $p = 3$ suffers a reversal in group velocity for $kd/\pi > 0.3$. These problems can be alleviated by either using a Shapiro filter to control the amplitude of short waves near the Nyquist cutoff or by periodic application of a non-linear normal mode initialization procedure (see Haltiner and Williams [4, pp. 392, 377]; Navon [21], Navon and de Villiers [6]). For Fig. 2b, this would imply a larger region of filtering outside the Nyquist cutoff region. As mentioned in Appendix B, in the 2-dimensional case this problem will be alleviated due to the faster geostrophic adjustment.

The results obtained in [6] show that in practice, for the 2-dimensional non-linear shallow-water equations, the case $p = 3$ is still useful. This is due to several reasons such as two dimensionality, "a posteriori" enforcement of the integral invariants conservation, and the use of the Shapiro filter.

Further research should consider extending the transfer functions analysis to the 2-dimensional shallow-water problem.

The process of geostrophic adjustment is known to work faster in a 2-dimensional domain because the gravity-waves spread their energy into a much larger

region during the same time period (see Appendix B). One can also consider the Turkel–Zwas scheme with $p > 1$ for staggered grid arrangement of the dependent variables, i.e., the C scheme of Arakawa and Lamb [1].

APPENDIX A

Here we obtain the inverse Fourier transform of $i\sigma/(\rho + \lambda^2\sigma^2)$ and $1/(\rho + \lambda^2\sigma^2)$. Following Schoenstadt [7] let us now consider:

$$\frac{1}{2\pi} \int_{-\infty}^{+\infty} \frac{e^{ikx}}{\rho + \lambda^2\sigma^2} \, dk, \tag{A1}$$

where

$$\rho = \frac{2 + \cos kp \, \Delta x}{3}, \tag{A2}$$

$$\lambda^2 = gH/f^2, \tag{A3}$$

$$\sigma = \frac{\sin kp \, \Delta x}{p \, \Delta x}. \tag{A4}$$

The denominator given by

$$\Psi = \rho + \lambda^2\sigma^2 = \left(\frac{2}{3} + \frac{1}{3}\cos kp \, \Delta x\right) + \left(\frac{\lambda}{p \, \Delta x}\right)^2 \sin^2 kp \, \Delta x \tag{A5}$$

is an entire function of k in the complex plane. The zeros of Ψ are now more complicated than in [7] and satisfy the equation

$$\cos kp \, \Delta x = \frac{1 \pm \theta}{2\xi}, \tag{A6}$$

where

$$\theta = \sqrt{4\xi(\xi + 2) + 1}, \tag{A7}$$

$$\xi = 3(\lambda/p \, \Delta x)^2. \tag{A8}$$

Let

$$k = k_r + ik_i, \tag{A9}$$

so we have

$$\cos(k_r + ik_i) \, p \, \Delta x = \frac{1 \pm \theta}{2\xi}. \tag{A10}$$

And by separating real and imaginary parts we obtain

$$\cos k_r \, p \, \varDelta x \cos ik_i \, p \, \varDelta x - \sin k_r \, p \, \varDelta x \sin ik_i \, p \, \varDelta x = \frac{1+\theta}{2\xi} \qquad \text{(A11)}$$

which can be written

$$\cos k_r \, p \, \varDelta x \cosh k_i \, p \, \varDelta x - i \sin k_r \, p \, \varDelta x \sinh k_i \, p \, \varDelta x = \frac{1\pm\theta}{2\xi} = \text{real.} \qquad \text{(A12)}$$

Thus

$$\cos k_r \, p \, \varDelta x \cosh k_i \, p \, \varDelta x = \frac{1\pm\theta}{2\xi},$$

$$\sin k_r \, p \, \varDelta x \sinh k_i \, p \, \varDelta x = 0. \qquad \text{(A13)}$$

Solving (A13) yields

$$k_r = \pm n\pi/p \, \varDelta x \qquad \text{(A14)}$$

or

$$k_i = 0. \qquad \text{(A15)}$$

By substituting in the first equation of (A13) we obtain

$$\cosh k_i \, p \, \varDelta x = (-1)^n \frac{1\pm\theta}{2\xi} \qquad \text{(A16)}$$

or

$$\cos k_r \, p \, \varDelta x = \frac{1\pm\theta}{2\xi}. \qquad \text{(A17)}$$
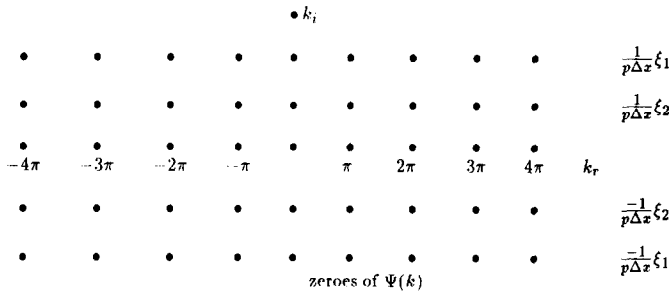
The only possible solutions of (A16)–(A17) are

$$k_r^n = \pm \frac{n\pi}{p \, \varDelta x},$$

$$k_i^n = \pm \frac{1}{p \, \varDelta x} \xi_1 \qquad (n \text{ even}), \qquad \text{(A18)}$$

$$k_i^n = \pm \frac{1}{p \, \varDelta x} \xi_2 \qquad (n \text{ odd}),$$

where

$$\xi_1 = \cosh^{-1} \frac{1+\theta}{2\xi},$$

$$\xi_2 = \cosh^{-1} \frac{\theta-1}{2\xi}.$$

(A19)

Thus all the zeros of the denominator lie off the real axis. However, the poles are not of the same imaginary part as in [7].

Since arc cosh z is an even function, the poles are located as follows:

At its zeros, it can be shown that all the zeros are simple and, moreover,

$$\Psi'(k) = \frac{ip\,\Delta x\theta}{3} \sin h\xi_1 \qquad (n \text{ even}),$$

$$\Psi'(k) = \frac{ip\,\Delta x(2-\theta)}{3} \sin h\xi_2 \qquad (n \text{ odd}).$$

(A20)

Consider the integral in Eq. (A1) which is an even function of x. Let $x > 0$. To ensure $\mathrm{Re}(ikx) < 0$, we will need $\mathrm{Im}(k) > 0$, i.e., we will close the contour in the $\mathrm{Im}(k) > 0$ half plane.

As long as we route the contour in the $\mathrm{Im}(k) > 0$ half plane to avoid all the poles, the integrand is exponentially decaying as $|k| \to \infty$. By using the residue theorem for $x > 0$, we obtain

$$\frac{1}{2\pi} \int_{-\infty}^{+\infty} \frac{e^{ikx}\,dk}{\rho + \lambda^2\sigma^2} = i \sum_{\mathrm{Im}(k) > 0} \mathrm{Res}\left(\frac{e^{ikx}}{\rho - \lambda^2\sigma^2}\right)$$

$$= i \sum_{\mathrm{Im}(k) > 0} \left(\frac{e^{ikx}}{\Psi'(k)}\right),$$

(A21)

where

$$\hat{k} = k_r^n + i k_i^n \qquad \text{given by (A18)} \tag{A22}$$

$$= \frac{3}{p\,\varDelta x} \left\{ \frac{1}{\theta \sinh \xi_1} e^{-x\xi_1/p\,\varDelta x} \right.$$

$$\left. + \frac{1}{(2-\theta)\sinh\xi_2} e^{-x(\xi_2 - i\pi)/p\,\varDelta x} \right\} \sum_{n=-\infty}^{\infty} e^{2ni\pi x/p\,\varDelta x}. \tag{A23}$$

In a similar fashion,

$$\frac{1}{2\pi} \int_{-\infty}^{+\infty} \frac{i\sigma e^{ikx}\,dk}{\rho + \lambda^2 \sigma^2} = i \sum_{\mathrm{Im}(k)>0} \frac{i\sigma(\hat{k})\,e^{ikx}}{\Psi'(\hat{k})},$$

$$= i \sum_{\mathrm{Im}(k)>0} \frac{i\sigma(\hat{k})\,e^{ikx}}{\Psi'(\hat{k})},$$

$$= 3 \left(\frac{1}{p\,\varDelta x} \right)^2 \left\{ \frac{e^{-x\xi_1/p\,\varDelta x}}{-\theta} + \frac{e^{-x(\xi_2 - i\pi)/p\,\varDelta x}}{2-\theta} \right\} \sum_{n=-\infty}^{\infty} e^{2ni\pi x/p\,\varDelta x}. \tag{A24}$$

The summations in Equations (A23)–(A24) are not a convergent series in the usual sense. These series can be viewed as the Fourier series for the function $S(x)$, periodic of period $p\,\varDelta x$ and given in the interval

$$\frac{-p\,\varDelta x}{2} < x < \frac{p\,\varDelta x}{2} \tag{A25}$$

by

$$S(x) = \sum_{-\infty}^{\infty} c_n e^{2ni\pi k/p\,\varDelta x}, \qquad c_n \equiv 1. \tag{A26}$$

But

$$c_n = \frac{1}{p\,\varDelta x} \int_{-p\,\varDelta x/2}^{p\,\varDelta x/2} S(r)\, e^{-2ni\pi x/p\,\varDelta x}\, dr = 1 \qquad \forall n. \tag{A27}$$

Thus

$$S(t) = p\,\varDelta x\, \delta(t) \tag{A28}$$

and its periodic extension becomes

$$S(x) = p\,\varDelta x \sum_{-\infty}^{+\infty} \delta(x - 2np\,\varDelta x). \tag{A29}$$

Thus, finally,

$$
\frac{1}{2\pi} \int_{-\infty}^{+\infty} \frac{e^{ikx}}{\rho + \lambda^2 \sigma^2} \, dk
$$

$$
= \left\{ \frac{1}{\theta} \frac{e^{-x\xi_1/p\Delta x}}{\sinh \xi_1} + \frac{1}{2-\theta} \frac{e^{-x(\xi_2 - i\pi)/p\Delta x}}{\sinh \xi_2} \right\} \sum_{-\infty}^{+\infty} \delta(x - 2np \, \Delta x). \qquad \text{(A30)}
$$

Similarly,

$$
\frac{1}{2\pi} \int_{-\infty}^{+\infty} \frac{i\sigma e^{ikx}}{\rho + \lambda^2 \sigma^2} \, dk
$$

$$
= \frac{3}{p\,\Delta x} \left\{ \frac{e^{-x\xi_1/p\Delta x}}{-\theta} + \frac{e^{-x(\xi_2 - i\pi)/p\Delta x}}{2-\theta} \right\} \sum_{-\infty}^{+\infty} \delta(x - 2np \, \Delta x). \qquad \text{(A31)}
$$

APPENDIX B

In this Appendix several concepts pertaining to geophysical fluid dynamics referred to in the paper will be defined in order to make the presentation self-contained.

B1. *The β-plane approximation*

The *beta*-plane approximation has to do with the spatial variation of the Coriolis parameter f. If one carries out a stereographic projection of points on the sphere, on a plane which is tangent at one of the sphere's poles, then the expansion of the Coriolis term $f = 2\Omega \sin \Psi$ in terms of the Cartesian stereographic coordinate y about $y = y_0$ yields

$$
f - f_0 + \frac{df}{dy} (y - y_0) + \cdots = f_0 + \frac{d}{dy} (2\Omega \sin \Psi)(y - y_0)
$$

$$
= f_0 + 2\Omega \cos \Psi_0 \frac{\partial \Psi}{\partial y} (y - y_0)
$$

$$
= f_0 + \frac{2\Omega \cos \Psi_0}{a} (y - y_0)
$$

$$
= f_0 + \beta_0 (y - y_0)
$$

$$
= f_0 \left[1 + \frac{\beta_0}{f_0} (y - y_0) \right], \qquad \text{(B1)}
$$

where

$$
\beta = \frac{2\Omega \cos \Psi}{a}, \qquad \text{(B2)}
$$

where a is the radius of the earth, Ω the angular velocity of the earth, and Ψ is the latitude.

Since we treat disturbances of scale L, it is reasonable to restrict the variation of f so that $|y - y_0| \lesssim L$. Since in mid-latitudes $\beta \sim f/a$, the second term in (B1) is bounded by

$$\left| \frac{\beta_0}{f_0} (y - y_0) \right| \leqslant \frac{L}{a} \tag{B3}$$

and, for geophysical applications, $L/a \sim 0.1$, so it is consistent to use $f = f_0$, except where f is differentiated and then we use Eq. (2).

The β-plane approximation was recognized by Rossby [17] as being sufficient to represent the effect of the variability of the Coriolis parameter.

B2. *Geostrophic Adjustment*

A major observed feature of atmosphere flow is the approximate balance in the horizontal plane (normal to gravity) of the Coriolis and pressure-gradient forces.

The issue of *geostrophic adjustment* is concerned with the mechanism whereby unbalanced fields of geopotential (mass) and momentum (wind) adjust or adapt to an ultimate state of geostrophic balance (Rossby [15], Obukhov [14], Blumen [11], Phillips [18], Cahn [16]).

In essence, the process of geostrophic adjustment takes place by means of wave propagation from local regions of initial imbalance, leaving behind a steady semi-geostrophic balanced flow, where

$$u = -gf^{-1} \frac{\partial h}{\partial y}$$

$$v = gf^{-1} \frac{\partial h}{\partial x}, \tag{B4}$$

h is the height field, and u and v are the zonal and meridional components of the velocity field. It has been shown by Cahn [16] that a sudden perturbation caused by an addition of momentum will cause the disturbance amplitude (from geostrophic balance) to first grow linearly with time, followed by a transition into an asymptotic state described by

$$\phi \sim \mathscr{I}_0(f_0 t) \sim (f_0 t)^{-1/2} \cos(f_0 t + \pi/4) \to 0 \tag{B5}$$

as $t \to \infty$. Here f_0 is the Coriolis parameter assumed constant, t is the time, and $\mathscr{I}_0$ denotes the zeroth-order Bessel function.

This is due to the fact that the initial imbalance excites short inertia-gravity waves that carry energy away from the initial region of imbalance.

Cahn [16] has shown that the disturbance energy propagates with the shallow-water speed

$$c = \sqrt{gH}, \tag{B6}$$

where H is the depth of the fluid and that the preexisting equilibrium state of the source region is reestablished in a period $T = 2a/c$, where $2a$ characterizes the dimensions of the region.

In two dimensions, Obukhov [14] has shown that the geostrophic adjustment solution is having the same qualitative asymptotic behavior as (B5); since the wave dispersion is isotropic, the disturbance amplitude ϕ tends now to zero as t^{-1}, (i.e., faster), as a consequence of the extra degree of freedom, i.e., two dimensions.

B3. Rossby Radius of Deformation

The Rossby radius of deformation is basically the horizontal scale at which rotation effects become as important as buoyancy effects in the rotating fluid called atmosphere. At small-length scales compared with the Rossby radius of deformation, the adjustment is the same as in a non-rotating fluid system; i.e., the pressure gradient is very large and gravity dominates the behavior of the system. For scales of length comparable to the Rossby radius of deformation, the Coriolis acceleration force becomes just as important as the pressure gradient term and thus rotation causes a response of the fluid—markedly different from the non-rotating case; i.e., it does not adjust to a state of rest, but rather to a state of geostrophic equilibrium. For the atmosphere the Rossby radius of deformation $\lambda = L_R$ is given by

$$\lambda = \frac{C_g}{f} = \frac{\sqrt{gH}}{f} = \frac{\sqrt{10.10^4}}{1.10^{-4}} \sim \frac{300}{10^{-4}} = 3.10^6 \text{m} = 300 \text{ km}, \tag{B7}$$

where g is the acceleration of gravity and H is the depth of the fluid (see Gill [12], Pedlodsky [13]).

B4. Staggered-Grid Systems

Grid-staggering is a procedure whereby discrete variables of different fields are located at alternate adjacent grid locations. The A-grid is a grid where all the variables are defined at the same grid location.

Grids B and C refer to different ways of distributing velocity and geopotential fields at adjacent grid locations.

Winninghoff [20] found that simulation of the geostrophic adjustment process with a finite difference scheme is highly dependent on the manner in which variables are distributed over the grid points.

For more detailed discussions see Arakawa and Lamb [1], Mesinger and Arakawa [19], and Haltiner and Williams [4].

REFERENCES

1. A. ARAKAWA AND V. R. LAMB, Computational design of the basic dynamical processes of the U.C.L.A. general circulation model, in *Methods in Computational Physics* Vol. 17 (Academic Press, New York, 1977), p. 174.
2. A. GADD, *Q. J. Roy. Meteorol. Soc.* **104**, 569 (1978).
3. A. GADD, *Q. J. Roy. Meteorol. Soc.* **104**, 583 (1978).
4. G. J. HALTINER AND R. T. WILLIAMS, *Numerical Prediction and Dynamic Meteorology* (Wiley, New York, 1980), p. 49.
5. D. C. JESPERSEN, in *Proceedings, AIAA 7th Computational Fluid Dynamics Conference, Cincinnati, OH, July 15–17, 1985*; 85-1493-CP.
6. I. M. NAVON AND R. DE VILLIERS, *Mon. Weather Rev.* **115**, No. 5, 1036 (1987).
7. A. L. SCHOENSTADT, *J. Comput. Phys.* **23**, 364 (1977).
8. A. L. SCHOENSTADT, NPS REPORT NPS-53-79-001, Naval Post-Graduate School, (unpublished).
9. A. L. SCHOENSTADT, *Mont. Weather Rev.* **108**, 1248 (1980).
10. E. TURKEL AND G. ZWAS, in *Proceedings, Third IMACS Symposium on Advances in Computer Methods for Partial Differential Equations*, edited by R. Vichnevetsky and R. S. Stepleman (Publications IMACS, Lehigh University, 1979).
11. W. BLUMEN, *Rev. Geophys. Space Phys.* **10**, No. 2, 458 (1972).
12. A. E. GILL, *Atmosphere-Ocean Dynamics*, International Geophysics Series Vol. 30 (Academic Press, New York, 1982).
13. J. PEDLOVSKY, *Geophysical Fluid Dynamics* (Springer-Verlag, New York, 1982).
14. A. M. OBUKHOV, *IZCV. Akad. Nauk. SSR. Ser. Geograph-Geofiz.* **13**, No. 4, 281 (1949).
15. C. G. ROSSBY, *J. Mar. Res.* **1**, 239 (1938).
16. A. CAHN, *J. Meteorol.* **2**, 113 (1945).
17. C. G. ROSSBY, *J. Mar. Res.* **2**, 38 (1939).
18. N. A. PHILLIPS, *Rev. Geophysics J.* **1**, 123 (1963).
19. F. MESINGER AND A. ARAKAWA, GARP Publishing Series Vol. 14 (WMO/ICSU Joint Organizing Committee, Geneva, 1976).
20. F. J. WINNINGHOFF, Ph.D. thesis, Department of Meteorology, University of California, Los Angeles, 1968 (unpublished).
21. I. M. NAVON, *J. Comput. Phys.* **52**, 313 (1983).
22. I. M. NAVON AND H. RIPHAGEN, *Comput. Geosci.* **12**, 129 (1986).